Heritage Science

RESEARCH

Open Access

Impacts of WWII bomb explosions on weathering damage of architectural heritage: Bath, England

Xiaoyu Wang[1*], Lisa Mol[2], Maurice Tucker[3], Tom Blenkinsop[4], Oscar Gilbert[5] and Oliver Campbell[4]

Abstract

The effects of bomb impacts, including the explosive force and combustion associated with these impacts, are preserved in only a few cities across the UK. In particular, World War Two (WWII) has left scars across a wide range of structures as a result of air raids. On immovable heritage, such as architectural structures, these impacts commonly take the form of craters, fractures and fire damage to stonework. This instantaneous damage is subsequently exposed to environmental stresses, such as moisture cycling, thermal stress and the movement of soluble elements and can thus lead to further deterioration of the stone. In this study, Rock Surface Hardness (RSH) measurements, permeametry measurements and microscopic observations were selected to capture stone deterioration data from 80-year-old bomb impacts on two walls of the Labour Exchange in Bath (UK) for spatial distribution analysis (Kriging) in Geographic Information Systems (GIS). The results show that the weathering forms that were found on the two walls can be attributed to nine different types. They can provide quantitative assessment of damage caused by bomb explosions and combustion in the war. The increase in permeability of walls and craters is shown to be primarily caused by the bomb explosion and combustion, whereas the decrease of hardness is associated with subsequent stone deterioration processes. This indicates that the interplay of initial damage likely accelerates subsequent response to environmental stress, extending the initial damage patterns from the impact crater to larger areas of stonework.

Keywords Bomb impact, Fire, Weathering damage, Craters, Bath city

Introduction

The Labour Exchange building in Bath is a Grade II listed building for the damage it received from the World War Two (WWII) Luftwaffe Baedeker air-raids on 25th to 27th April 1942 (Fig. 1). As Fig. 1 shows, the structure originally comprised a two-story building with a pitched roof, constructed of Bath Stone. Bath stone is an oolitic limestone comprised of ooids and bioclastic grains [2, 3]. Its honey colour gives the World Heritage City of Bath, England, a distinctive appearance.

Bombs are a form of damage to the built environment resulting from air-raids and the use of ground-based explosive devices. Bomb shrapnel impacts on stone buildings result in surficial cratering, fracturing and changes to material properties, such as permeability and surface hardness. In-situ measurement of stone properties is therefore highly desirable for heritage conservation efforts, but it is generally restricted to non-destructive testing [4–6]. Evidence of the active targeting of sites, as well as collateral damage when heritage is caught in war, is widely visible around Europe and farther afield

*Correspondence:
Xiaoyu Wang
704216608@qq.com
[1] School of Architecture and Civil Engineering, Shenyang University of Technology, Shenyang 110870, China
[2] Department of Geography and Environmental Management, University of the West of England, Bristol BS16 1QY, UK
[3] School of Earth Sciences, University of Bristol, Bristol BS8 1EJ, UK
[4] School of Earth and Environmental Science, Cardiff University, Cardiff CF10 2AT, UK
[5] Institute of Physics Publishing, Bristol BS2 0GR, UK

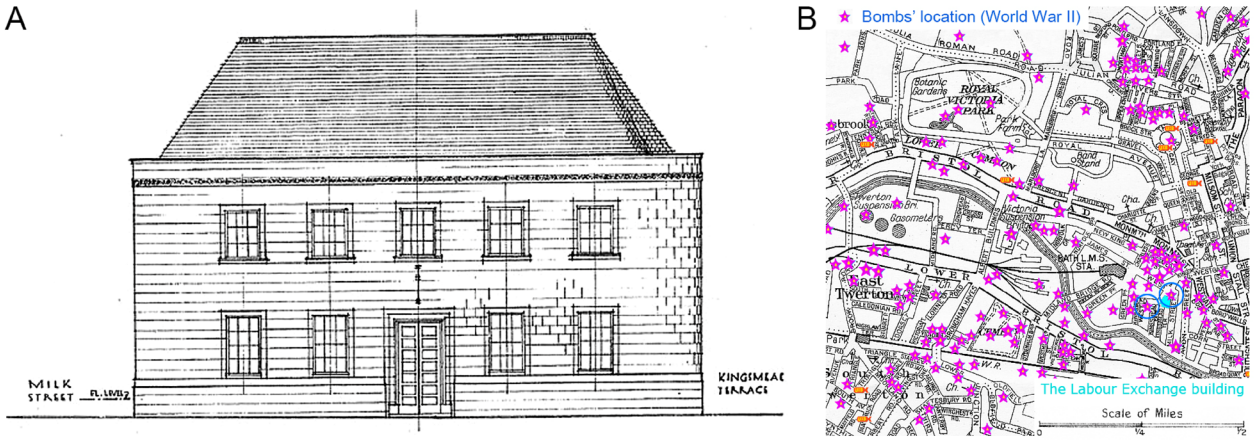

Fig. 1 **A** Labour Exchange building in Bath in 1942. **B** The location of WWII bombing incidents in Bath and the location of impact sites near the Labour exchange (2 blue circles) [1]

[7] which leaves a significant number of heritage sites exposed to potentially accelerated deterioration. When the detonation pressure wave, heat and shrapnel impact the walls of a building, stress generated by the explosion impacts travels through the surface and causes changes in the stone structure radiating from the initial impact zone. This stress dissipation pattern can cause widespread subsurface structural damage through fracture network development, as well as compaction at the direct impact point of the shrapnel, followed by loss of matrix density in the surrounding stone area. These fracture networks do not only deteriorate the strength of the stone at the time of impact but can also be exploited by weathering processes for more rapid deterioration of the stone on the medium- and long-term [7–9]. Bomb explosion impacts cause grain fracture directly below the impact, increase surface permeability and reduce surface hardness around the impact [10–12]. However, there are few studies on the long-term quantitative effects of this form of damage, especially in natural stone that typifies culturally important sites [13, 14]. Furthermore, in the case of heritage sites the impacted stonework is often friable due to decades, centuries or even millennia, of exposure to environmental stress such as moisture and temperature cycling, as well as movement and deposition of soluble components such as salts. Field instruments such as surface hardness probes and permeameters, as well as microscopic observation can provide valuable information on stone conditions which do not necessitate destructive approaches such as sampling of the materials or resistance drilling.

The aim of this study is to provide a quantitative assessment of stone deterioration associated with bomb explosions, particularly in the context of sites of cultural heritage. In view of the sensitive nature of heritage sites, methods of study need to be fully non-destructive and appropriate for in-situ quantitative analysis. To this end, this study utilises RSH (rock surface hardness) measurements, permeametry measurements and microscopic observation to capture data in situ. These data then facilitate further spatial analysis (Kriging) in Geographic Information Systems (GIS).

Methods

Survey preparation

Bath's Labour Exchange Building retains two explosive-damaged walls: the one facing James Street West and the other one facing Kingsmead North (Fig. 2). In April 1942 a bomb was dropped in the square directly adjacent to the Labour Exchange, which caused considerable cratering to both sides of the exposed building. While much of the building was demolished due to the extensive damage, these two outer walls were retained in a subsequent regeneration of the building. This provides the opportunity to study the effects of 80 years, almost to the day at time of measurement, of damage exposure to environmental stress, by a comparative study of impacted and non-impacted stonework.

The in-situ survey included a weathering forms survey, rock surface hardness (RSH) measurements, permeability measurements and infield microscopic observation, all of which are non-destructive techniques suitable for this type of heritage site. This was complemented with a photogrammetry-based survey. First, a full survey of the weathering features, including discolouration, flaking and crumbling, was carried out across the two walls (Fig. 3). These walls were then divided into a 180-square grid (30 horizontal and 6 vertical) to facilitate systematic

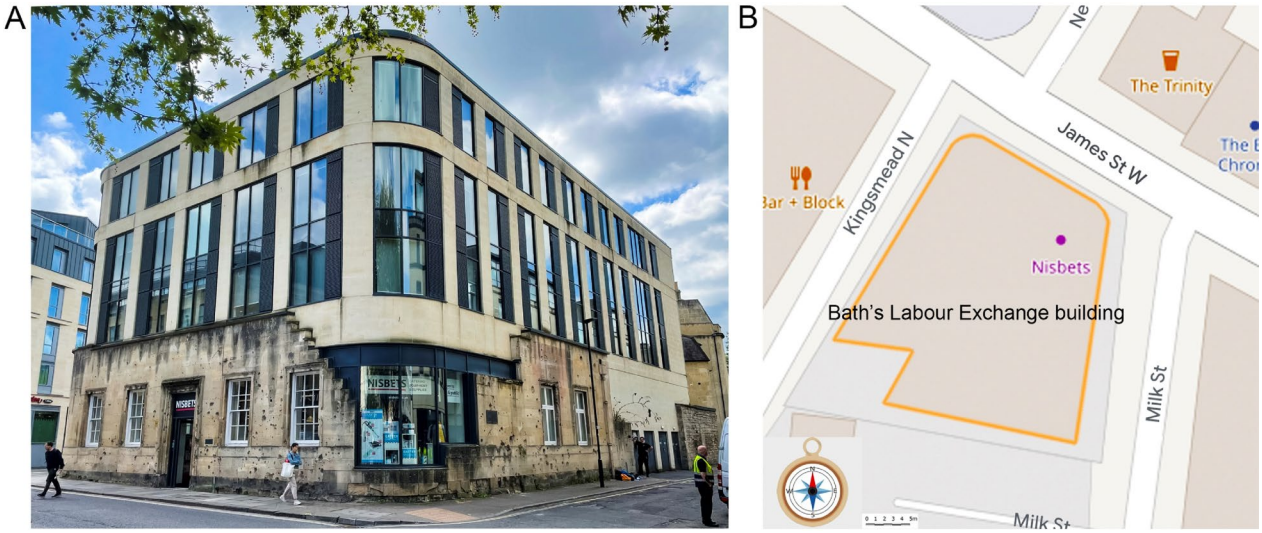

Fig. 2 **A** Labour Exchange building in Bath in 2022. **B** Geographical location of the building in Open Street Map [15]

measurements of rock surface hardness (RSH) and permeability across both impacted walls. Because the building components in the corner of the building were destroyed by the bomb, a total of 123 cells were measured on two walls finally (Fig. 4A). Ten representative craters were selected and each crater had 7–15 test points for hardness and permeability measurements (Fig. 7A).

Rock surface hardness (RSH) survey

As several studies have demonstrated [10, 11, 16, 17], RSH can be used as a key-indicator of the degree of weathering of a surface. In this study, an Equotip 3 with D-type probe was used to map differences in RSH across the experiment sites. This equipment was originally developed for the testing of metals [12], but it is now used in both natural settings [18, 19] and the built environment [20]. The surface hardness is measured through rebound of a 3 mm diameter spherical tungsten carbide test tip against the rock surface. This tip is mounted in an impact body and impacts under spring force against the test surface from which it rebounds [21]. The velocity before impact (V′) and after impact (V2) are measured automatically and displayed as a ratio ($V2/V' \times 1000$) which is denoted by the unit 'L', or Leeb unit [22].

As noted by Hansen et al. [23] repeated rebound tests at the same location on the rock surface result in an artificial increase in rebound strength due to compaction of the surface by the rebound device. To minimize this effect and to avoid artificial compaction of the surface, measurements were taken within a 10 cm × 10 cm space, but never on the same position, after manually cleaning the surface of debris such as mud and grit, deposited by wind and surface runoff. This test was repeated 15 times on each cell of two walls to map variability in RSH with a total of 1845 impact measurements. Using the same method, five RSH measurements were made at each test point of each crater, in total 545 impact measurements for craters. By calculating both the mean value per section measured and the standard deviation, the weathering progression was estimated at all test sites.

Air permeametry survey

Air permeability plays an important role in understanding the air transport behaviour in weathered rocks, and is an indicator of effective permeability, which in turn facilitates the movement of solutes through a porous stone. An air permeameter is essentially a compressed gas or vacuum cylinder through which gas can be released into or extracted from a porous media. Compressible, impermeable material is placed at the permeameter tip to prevent leakage from between the cylinder outlet and the porous medium. Gas flow rate and gas pressure are monitored and can be transformed into gas permeability using a modified form of Darcy's law with a geometrical factor depending on tip seal size, as proposed by Goggin [24].

The permeability of the sample's surface was investigated using a New England Research TinyPerm3 air Permeameter. This instrument assesses air permeability of the stone by creating a vacuum through a piston stroke, drawing air from the sample. The instrument monitors the volume of air withdrawn, and the transient vacuum pulse created at the surface. These data are computed by the instrument and converted into a permeability value in Darcys (D) [25]. The instrument was calibrated using the manufacturer's standards. As with the RSH readings,

Fig.3 **A** Main weathering forms of two walls: **B** moist zones. **C** crack. **D** spalling. **E** staining. **F** crust. **G** encrustration. **H** higher plants. **I** lichens. **J** mosses

the permeability of each cell of two walls was measured three times, totally 369 measurements for the two walls. The permeability of each test point of each crater was measured once, totalling 109 measurements for craters. It should be noted that as air permeability values have been shown to differ significantly from water permeability values [26], the permeability results presented here serve only to highlight relative differences across the sample, and cannot be used to accurately describe the likely ingress of water as a weathering agent [27]. The measurements are therefore used as a measure of relative susceptibility of the stone to deterioration stresses due to loss of density and/or crack formation.

Microscopic observation

To study rock surface microtopography, in-situ microscopic observations were carried out using a Bysameyee USB Digital Microscope, Handheld 40×-1000× Magnification Endoscope. Eight different areas of two walls were observed, including freshly exposed surfaces above the lead damp course, just outside impact craters, fire damaged window frames, front corner 'discoloured' blocks, inside small craters, inside a large impact crater, large scale area of deterioration at bottom of the wall, the rock surface change where microbes-algae had colonised, giving a total of 40 photomicrographs for two walls. These images informed the assessment of likely drivers of deterioration across individual crater points (Fig. 9A).

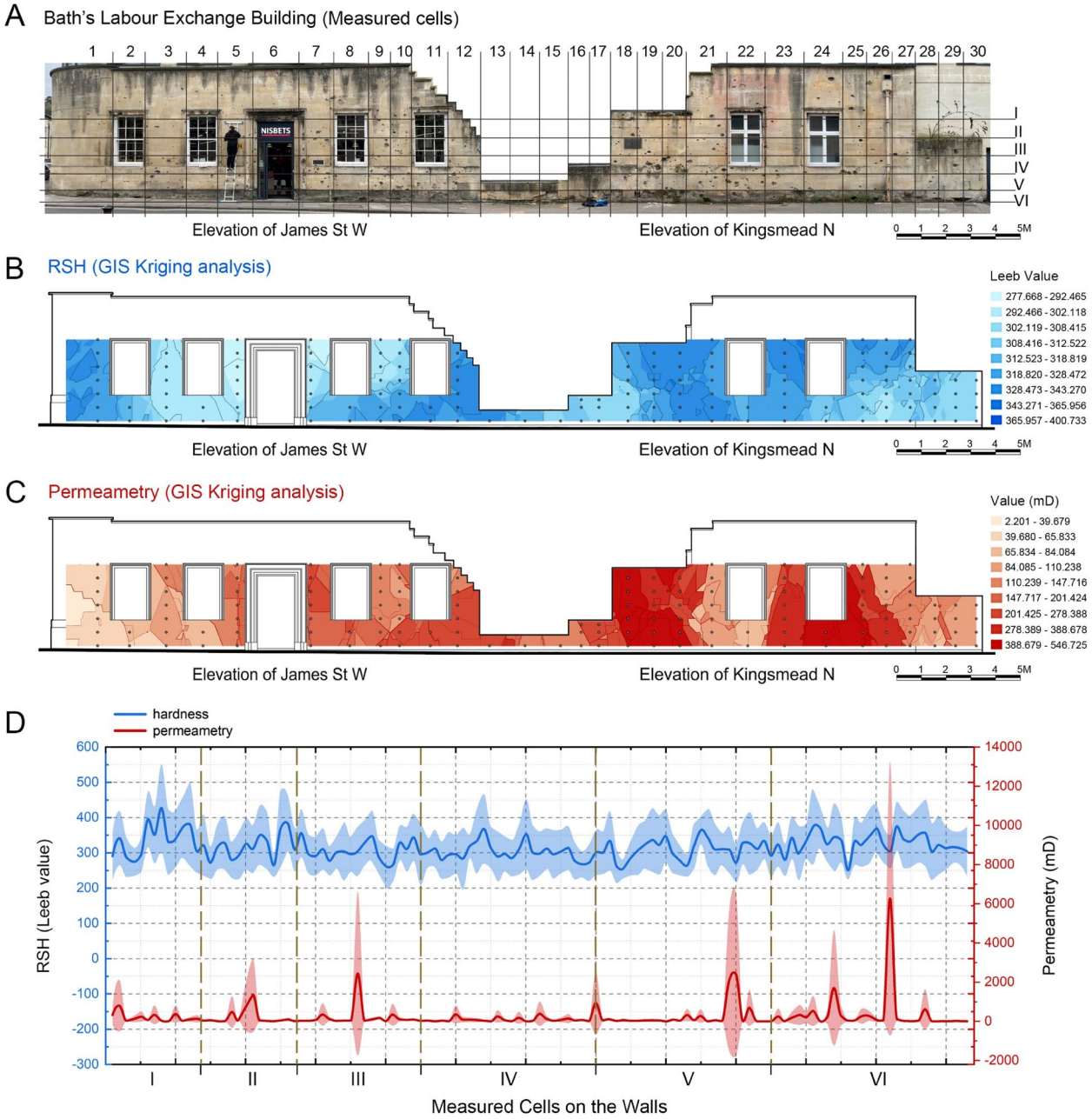

Fig.4 **A** 30 horizontal partitions and 6 vertical partitions on the two walls for measurements. **B** RSH (GIS Kriging) analysis. **C** Permeametry (GIS Kriging) analysis. **D** RSH and permeametry survey data of two walls

Spatial distribution analysis (Kriging) methods

Kriging, a geostatistical interpolation method that involves calculating the distance between objects and their spatial correlation was adopted here to inform likely RSH and permeability patterns across the surface [28, 29]. Kriging is an alternative to many other point interpolation techniques. Unlike straightforward methods, kriging is based on a spatial regression of samples collected from a spatial domain. Such methods are called forward geostatistical methods [30]. Kriging is an exact interpolation estimator used to find the best linear unbiased estimate. Detailed discussions of kriging methods and their descriptions can be found in Goovaerts, Webster [31]. The Kriging method can classify and partition the measured data for analysis and discussion.

In this study, RSH and permeametry mean data were processed in an ArcGIS Pro Geographic Information Systems software package, with each cell shown in Fig. 4 given a point with a RSH or permeability value. Then, the Kriging (Spatial Analyst) interpolation method was used to find out other predictive RSH and permeametry values and spatially analyze the data that covered the entire study area, to obtain an estimate of the value between sample points within the specified study area. The results were contoured. The same methods were used to analyze the spatial distribution of RSH and permeability at test points in each crater.

Results

Weathering forms

A visual survey of weathered forms on two walls of Bath's Labour Exchange Building is presented in Fig. 3. Weathering forms refer to the weathering phenomena visible on the centimetre to metre scale. The standardized classification scheme of weathering forms by Fitzner and Heinrichs [32] was used for mapping the spatial distribution and diversity of weathering morphology and intensity.

The weathering forms that were found on the two walls can be attributed to nine types, divided into two general groupings: (1) physical deterioration including: "Moist zones", "Staining", "Spalling", "Encrustration", "Crust", "Crack", and (2) biological deterioration including "Higher plants (e.g. grasses, saplings, or larger vegetation)", "Lichens" and "Mosses" [33] (Table 1). Table 1 also shows the distribution areas of final damage categories investigated.

Rock surface hardness (RSH) survey results

As shown in Figs. 4B, D associated with Fig. 5A, the RSH values of 123 cells of the two walls range from 200 to 592 L (Leeb values). The cells with low hardness values

Table 1 Main weathering forms and distribution areas

Weathering forms	Distribution areas
Moist zones	Distributed on the top and bottom walls of the building
Staining	Mainly on the upper wall facing Kingsmead N Street
Spalling	Mainly distributed around the crater and the bottom wall
Encrustration	Mainly on the upper wall facing Kingsmead N Street, and on the left wall of the opening of the door facing James St W
Crust	Mostly inside the crater, and on some blackened walls
Crack	This weathering form exists on two walls of the whole building
Higher plants	Distributed on the bottom walls of the building
Lichens	Distributed on the bottom walls of the building
Mosses	Distributed on the windowsill at the corner of the building

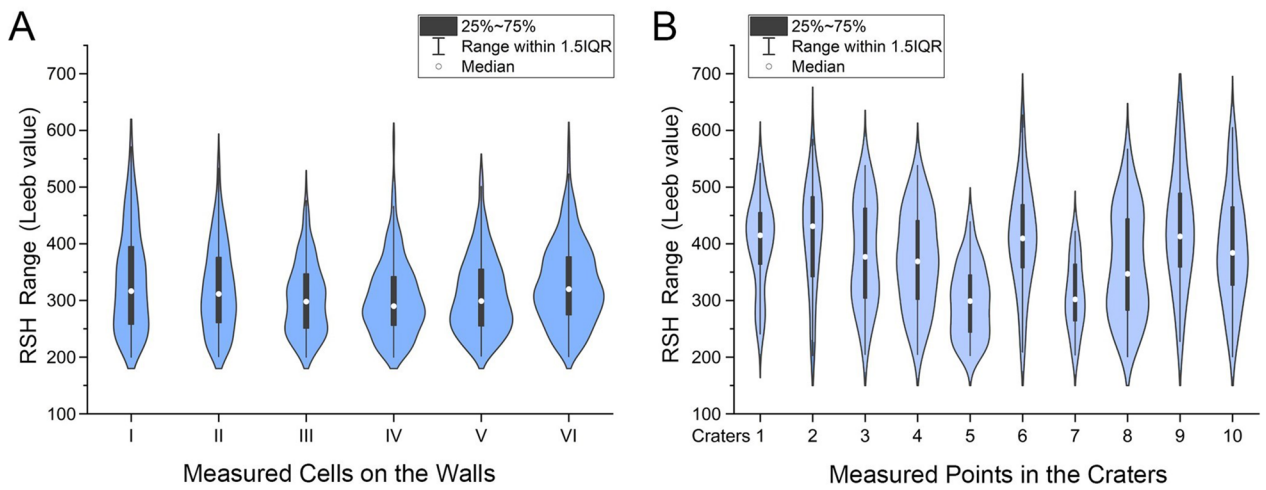

Fig.5 **A** The density and distribution of RSH data of the two walls. **B** The density and distribution of RSH data of ten craters

are mainly located near doors and window openings, the cells near the ground floor, and the walls at the corners of the building. The cells with higher hardness values are mainly distributed on the upper part of the wall, far from the ground. The mean RSH values of the III, IV, V vertical partitions on the wall are about 20–30 L lower than other partitions. However, the standard deviation of I, II, VI vertical partitions are obviously larger than those of the III–V vertical partitions, and although the minimum RSH values of the three partitions are almost the same. The maximum RSH values range from 613 to 501. III–V vertical partitions are the areas where the windows and doors were missing due to direct exposure to the explosion and ensuing fire damage.

As shown in Figs. 7, 8 associated with Fig. 5B, the RSH values of ten craters range from 201 to 650 L. Craters 3, 4, 5, 7, 8, and 10 all gave lower hardness values, and each crater presents a comparison of hardness values. Except crater 5, the mean RSH value of other craters is greater than the mean RSH value of each cell of two walls.

Air permeametry survey results

As shown in Figs. 4C, D associated with Fig. 6A, the permeametry values of 123 cells of the two walls range from 0.0024 to 13,800 mD. The cells with large permeability are mainly distributed in the partition VI which is closest to the ground, near the openings of doors and windows, and near the wall where the bomb exploded on the ground. The cells with low permeability are mainly distributed in the walls that are relatively continuous, without openings, and are higher from the ground. This indicates that the bomb explosion and the location of water penetration into the wall are the main factors affecting the permeability value. On the one hand, they are most affected by the bomb explosion; on the other hand, groundwater penetrates into the lower walls. The upper walls have rainwater penetrating into the wall, so that their permeability values are greater than that of partition IV. Therefore, the permeability value is the order of the bomb explosion's impact + groundwater impact + rainwater impact.

As shown in Figs. 7, 8 associated with Fig. 6B, the permeametry values of ten craters range from 2 to 13,300 mD. Craters 2, 4, 5, 7, 8, and 10 show very large permeability values, and each crater presents a comparison of permeametry values. The mean permeability values of craters 2, 4, 5, 7, 8, 10 are also greater than the mean permeability value of each cell of two walls.

Spatial distribution analysis (Kriging) methods

For the purpose of understanding the spatial distribution regularities of the RSH and permeametry mean data, the kriging interpolation method of the geostatistical module in ArcGIS Pro was used to assess the RSH and permeametry concentrations on each cell of two walls. Based on this, a spatial distribution map of the RSH and permeametry concentrations on two walls was created. Figures 4B and C show an increasing or decreasing trend, and all these attributes have obvious high-value and low-value areas. There is an obvious large area of low-value RSH area at the openings of the door and windows of the wall facing James St W, and two high-value RSH areas at both corners of the wall. The two low-value RSH areas on the wall facing Kingsmead N are near where two walls were badly damaged in the war, and the high-value RSH area is on the upper wall (Fig. 4B). In general, the permeability of the wall facing Kingsmead N is greater than that of James Street W, and the permeability of the lower walls is greater than that of the upper walls (Fig. 4C).

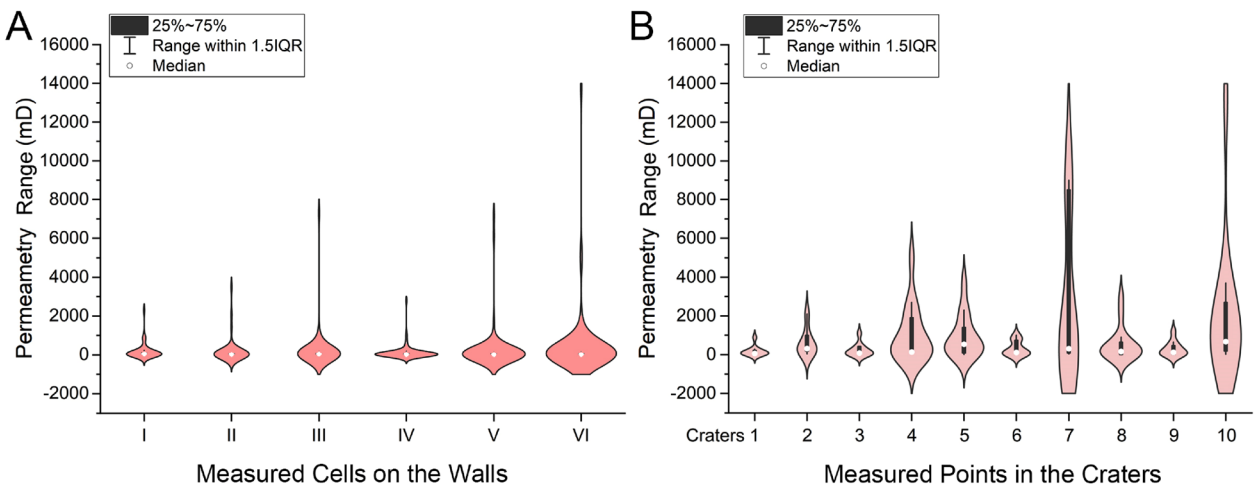

Fig.6 **A** The density and distribution of permeametry data of the two walls. **B** The density and distribution of permeametry data of ten craters

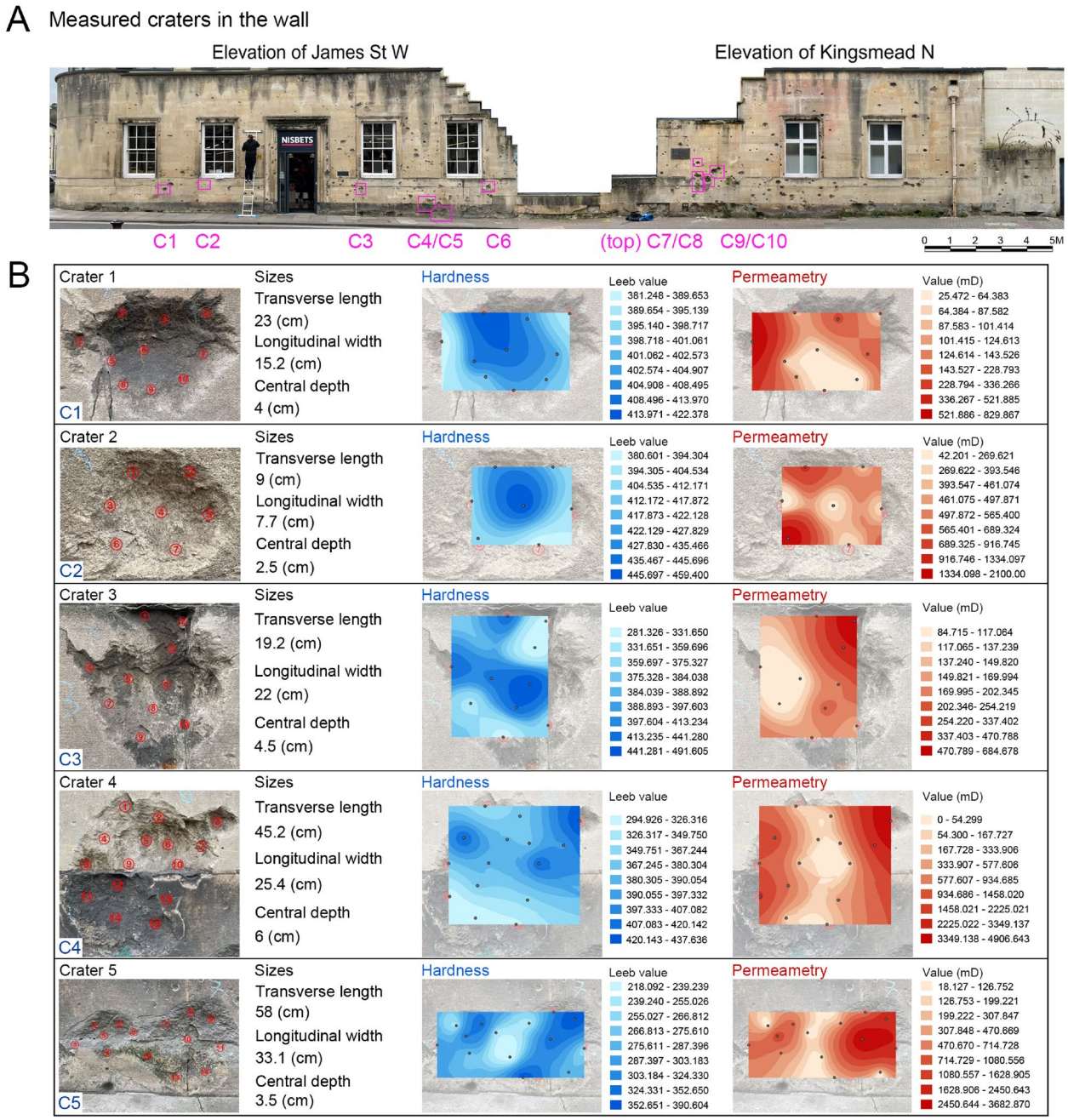

Fig.7 **a** Ten craters for measurements. **b** RSH and permeametry (GIS Kriging) analysis for crater1 to crater5

As shown in Figs. 7B and 8B, The RSH and permeability values do not seem to be consistently distributed within the craters. But in some craters, the RSH value of the middle of a crater is greater than that of the edge. The permeability value of the edge of a crater is greater than that of the middle. If the crater is cracked or spalling, the permeability can be very high.

Microscopic observations

Microscopic observation is the most suitable method for non-destructive testing of architectural heritage. Bath stone is the material of the exterior wall of Bath's Labour Exchange Building. Bath stone is an oolitic limestone comprised of ooids and bioclastic grains, and under the microscope, the sub-mm ooids are spherical grains composed of calcite [34].

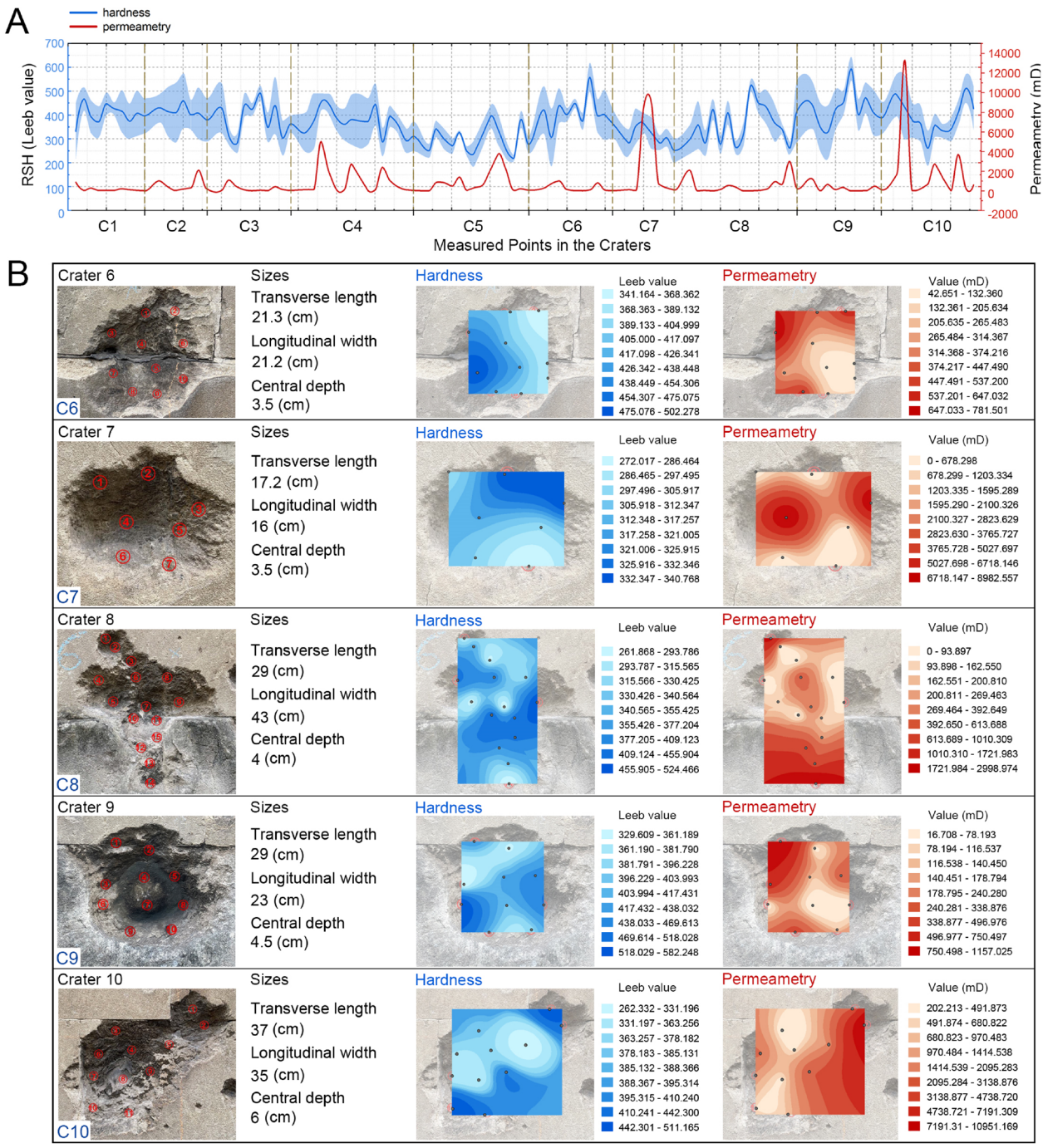

Fig.8 **a** RSH and permeametry survey data of the craters. **b** RSH and permeametry (GIS Kriging) analysis for crater6 to crater10

Figure 9B shows the eight areas observed. Site 1 is a freshly exposed surface of stone unaffected by impacts; ooids are clearly visible with no signs of etching or pitting; it looks a fresh, unweathered surface. There is little microporosity; the limestone is tight. A few likely microbial filaments (dead) occur on the surface. Site 2 is outside of the craters, with well-preserved grains, no porosity, and some etching of the ooids. Site 3 is a fire-damaged window frame, with a pink-red staining of some grains wherein the iron would be located. Some etching of grains. Site 4 is from a discoloured stone on the front corner and shows a surface with a pale encrustation with

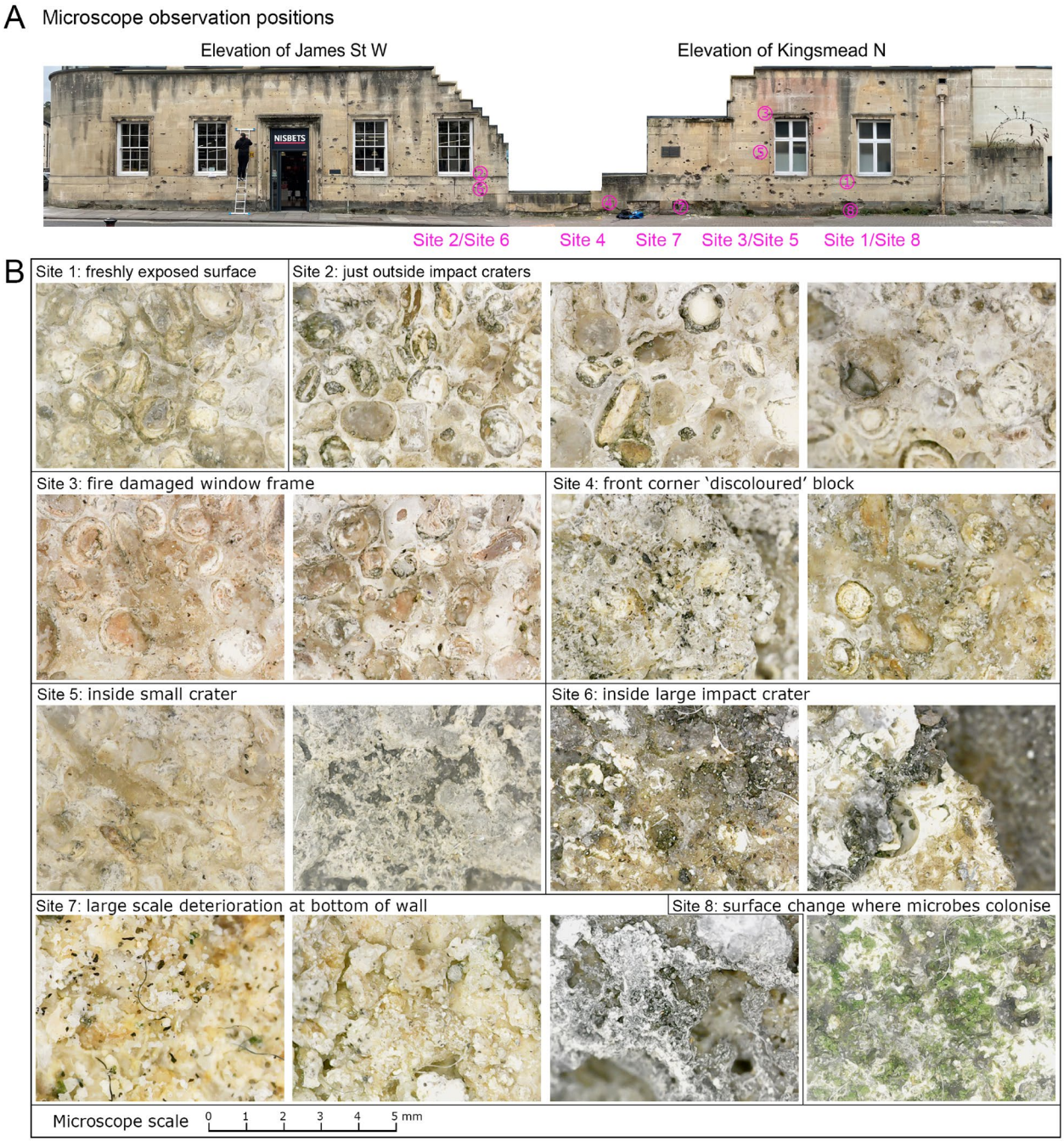

Fig.9 **a** The position of the microscope observations. **b** Microscopic observations of different areas of the building

fine black particles and some faint pink colouration from fire damage. Site 5 is the inside of a small crater, where few ooid grains are visible, and there is a cream-coloured crust/coating with dark areas, probably from weathering and microbial encrustation. Site 6 is inside a large impact crater, where the surface has been weathered and coated so few grains are visible. Site 7 from the bottom of the wall near the right edge of the information plaque shows the effects of long-term exposure to weathering, with a flakey appearance and dark particles, probably from air pollution and microbial encrustation. The two left images look like comminuted rock with microclasts on the surface, possibly powdered rock from an impact. Site 8

shows a rock surface with a green colour from a biofilm of cyanobacteria–algae.

Discussion

The power of a bomb explosion to destroy architectural heritage is staggering [35, 36]. Architectural heritage that survives a war and bomb damage continues to be exposed to the sun, frost, damp and other environmental stresses. But a single bomb attack can do as much to weather a building as thousands of years of sun and freezing combined. Bomb explosions cause craters and fractures in a building's walls. On the wall facing James Street West, there are about 80 visible craters of different sizes and depths, visible area of crater/wall area = 7.7%; on the wall facing Kingsmead North, there are about 60 visible craters of different sizes and depths, visible area of crater/wall area = 11.5%. Cracks will inevitably develop over time, leading to an increase of the permeability coefficient and permeability generally. The RSH and permeametry will differ radically based on the proximity of impacts as well as deterioration associated with ground water rise up to the lead line. In the case of the Bath Labour Exchange, the permeability of the wall stones can be compared from the data in Fig. 4D, which show that the minimum permeability value is 0.0024 mD and the maximum permeability is 13,800 mD. The RSH measurements can be used to determine relative deterioration of the surfaces. As Fig. 4D shows that the minimum value of the walls is 200 L and maximum value of is 592 L. It is possible that fractures resulting in a discernible reduction of hardness in the stone have wider micro-fracture networks associated with them [7, 9].

After the bomb exploded at ground level, some of the shrapnel hit the wall, on the one hand, causing a strong impact, forming many craters; on the other hand, the bomb carried burning material, causing the wall to be affected by fire [37, 38]. As shown in Figs. 5 and 6, bomb explosions and combustion are the main factors affecting the loss of RSH and enlargement of pore-size of the craters. According to the field investigations and measurements, some of the wall craters are caused by shrapnel directly impacting the wall, and some are caused by other objects hitting the wall of the building due to the formation of fragments caused by the explosion. The high RSH-value areas of two walls are distributed on the upper wall facing Kingsmead N, and under the window near west corner of the wall facing James St W. The low RSH-value areas were distributed at the openings of the door and windows of the wall facing James St W, and near the corner of the wall facing Kingsmead N. The high permeametry-value areas of two walls were distributed on the lower wall facing Kingsmead N, and near the corner of the wall facing Kingsmead N. The low permeametry-value areas were both distributed at east corner of the wall facing James St W.

Architectural heritage after a bomb explosion is more prone to weathering problems (Fig. 10A). These are mainly the results of bomb explosion and combustion, as well as later pollution and weathering. As shown in Figs. 3 and 10B, the common forms of weathering are cracks, spalling, staining and biological growth. This is because the explosion has a great impact force, resulting in loose texture, reduced hardness, increased permeability of the Bath stone, and a greater susceptibility to weathering and disintegration in water. Under the action of the external environment for a long time, the internal physical stress of the stone is unevenly distributed. Small cracks form first in the stone, and then these extend to create longer cracks [39, 40]. With a larger area of cracks, the surface stone is subjected to spalling. At the same time, when the humidity reaches a certain level, liverworts and even more substantial plants may grow in cracks.

At the same time, combustion after an explosion is another main reason for the formation of a loose, porous texture, reduced hardness and increased permeability of the Bath stone. Burning at high temperatures can also cause thermal cracking of rocks [41]. As shown in Fig. 9B, according to the microscope study, the main component of the Bath stone is calcite, and its honey colour is related to the presence of iron oxides-hydroxides (goethite–limonite), derived from the oxidation of pyrite [2, 8]. Calcite (calcium carbonate) is insoluble in neutral pH water but is affected by more acidic water, such as rainwater, which causes etching of the limestone. On being heated, as in a fire, calcite can decompose: $CaCO_3 = CaO + CO_2\uparrow$ [42, 43], making the limestone readily affected by further weathering by rain and frost. The staining of buildings is also related to explosions and post-explosion combustion (Fig. 3). Bomb explosions can generate temperatures up 5000 °C; the presence of hydrated iron oxides in Bath stone are altered to ferric oxide (Fe_2O_3), giving the building walls a reddish-pinkish stain. A temperature higher than 1300 °C favours the oxidation of hydrated iron oxides to ferric oxide (Fe_2O_3) [42, 43].

It is also interesting to note that there are many craters in which the hardness of the inner centre is higher than that of the crater edge, and the permeability of the inner part is lower than that of the crater edge (Fig. 10B). This phenomenon is referred to as Reverse Weathering [44–46]. A (black) crust can occur on lime containing materials in the presence of SO_X (e.g. from pollution) leading to a transformation of calcite into gypsum. The crust can acquire a blackish colour, due to encapsulation of dirt and soot into gypsum. The chemical equation for the formation of the crust is $CaCO_3 + H_2O + H_2SO_4 = CaSO_4 \cdot 2H_2O$

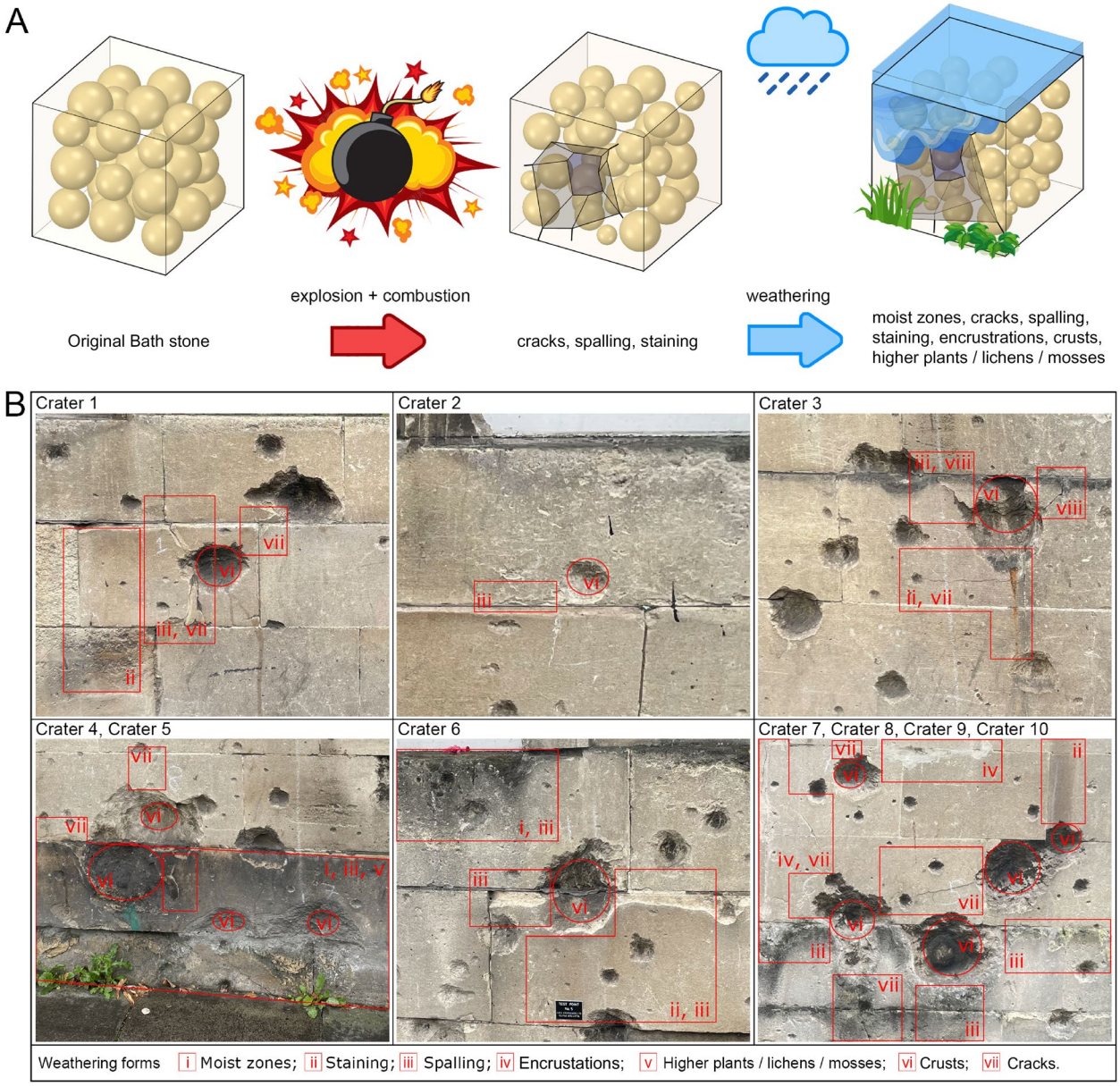

Fig. 10 **a** The architectural heritage that survived the war, though exposed to the sun, freeze-thaw and other forces. However, a single bomb attack can do as much to weather a building as thousands of years of sun and freeze-thaw combined. **b** Weathering forms inside the craters

(gypsum) + CO_2↑ [42, 43]. According to Stephenson's theory, a thin film of water formed by condensation can hold more dust particles with polluting properties, such as sulphur dioxide, together [47, 48]. The speed of dust concentration depends on the temperature difference between the wall and the air in contact with it. Thus, we find that the most frequent crusts are found in cold, wet craters where water is easily condensed. The black crust continues to feed more gypsum into the porous rock further inside the crater, and the gypsum continues to invade deeper into the rock. With the increase in the thickness of the gypsum layer, the crater has a layer of reverse weathering crust inside, and it is more difficult to be weathered (Fig. 10B). Encrustation also takes place locally on Bath stone in damp areas, as a result of microbial activity and the presence of a biofilm; these are mostly grey crusts of thin, crinkly calcite. Both gypsum and calcite crusts and efflorescent, as well as green microbial-algal growths, can develop near the ground of Bath stone buildings as a result of rising damp.

Conclusions

Heritage and cultural buildings are at risk from conflict damage in many parts of the world and Bath provides one example of a city where most of the evidence of the extensive WWII damage has been removed with just one clear example of a building (the former Labour Exchange) with shrapnel damage tastefully preserved as a memorial to those dark days of April 1942 [1, 2].

The explosion and combustion of a bomb make the rock of the wall disintegrate and break under the physical and mechanical action, and this process is the process of physical weathering. Later in the next few decades, rain, pollution, plant growth, processes of chemical and biological weathering are added [42, 43]. Whether it is a large crater or a small crack, it is an important factor causing damage to the architectural heritage [7–9]. In this study, In-situ measurements combined with spatial distribution analysis (Kriging) in GIS, RSH (rock surface hardness) and permeability spatial distribution maps of two walls and ten craters were produced. The micro-damage to the walls of the building from the bomb explosions has been examined by microscopic observation. It can be concluded that for the wall with more cracks (visible and invisible), weathering is more serious from a quantitative assessment of damage caused by bomb explosions in WWII [11, 12]. The increase of permeability of walls and craters was mainly caused by bomb explosions and combustion, while the decrease of hardness is more affected by later weathering. This indicates that the interplay of initial damage likely accelerates subsequent response to environmental stress, extending the initial damage patterns from the impact crater to larger areas of stonework [13, 14, 38].

Eighty-year (from 1942 to 2022) weathering and degradation are no match for the destruction of the architectural heritage by a single night of aerial bombing.

Abbreviations

RSH	Rock surface hardness
GIS	Geographic information systems
WWII	World War Two

Acknowledgements

The authors are grateful to James Queay, for the in-situ permeability measurements in April, 2022. The authors would like to thank Professor Elizabeth Laycock (Sheffield Hallam University) and the anonymous reviewer, for providing information on the website.

Author contributions

Xiaoyu Wang wrote the manuscript, carried out in-situ hardness measurements, mapping and drawing of the architectural heritage; Lisa Mol edited the manuscript, conceived and organized the in-situ measurements, and conducted on-site microscopic observations; Maurice Tucker edited the manuscript, analyzed and wrote the results of microscopic observations; Tom Blenkinsop edited the manuscript and provided helpful comments; Oscar Gilbert took photos on the spot for the analysis of weathering forms; Oliver Campbell provided helpful suggestions. All authors read and approved the final manuscript.

Funding

This research was funded by Leverhulme Trust Research Grant RPG-2017-408, National Natural Science Foundation of China (Project No: 51978417), China Scholarship Council (File No. 202108210150).

Availability of data and materials

The data are available within the article.

Declarations

Ethics approval and consent to participate

Not applicable.

Consent for publication

Written informed consent for publication was obtained from all participants.

Competing interests

The authors declare that they have no competing interests.

Received: 17 March 2024 Accepted: 26 April 2024
Published online: 16 May 2024

References

1. Bath Blitz Memorial Project. Maps of bomb locations. Bath Heritage Watchdog 2022. http://www.bathheritagewatchdog.org/bathblitz/topmap.htm.
2. Tucker ME. Impact marks on Bath stone (Jurassic oolite): ww2 bomb and bullet damage on buildings in Bath. J Bath Geol Soci. 2021;39:30–7.
3. Tucker ME, Brisbane M, Pitman D, Kearn O. Source of Roman stone for Aquae Sulis (Bath, England): field evidence, facies, pXRF chem-data and a cautionary tale of contamination. Geol Curator. 2020;11(3):217–30.
4. Allen CD, Ester S, Groom KM, Schubert R, Hagele C, Olof D, et al. A geologic assessment of historic saint elizabeth of hungary church using the cultural stone stability index Denver, Colorado. Urban Geomorphol. 2018;14:277–302.
5. Hatır ME, İnce İ, Korkanç M. Intelligent detection of deterioration in cultural stone heritage. J Build Eng. 2021;44: 102690.
6. Pope GA, Meierding TC, Paradise TR. Geomorphology's role in the study of weathering of cultural stone. Geomorphology. 2002;47(2–4):211–25.
7. Mol L, Gomez-Heras M. Bullet impacts and built heritage damage 1640–1939. Herit Sci. 2018;6:35.
8. Mol L. Armed conflict impacts on the microscale. J Phys: Conf Ser. 2017;902: 012032.
9. Mol L, Clarke L. Integrating structure-from-motion photogrammetry into rock weathering field methodologies. Earth Surf Proc Land. 2019;44(13):2671–84.
10. Betts MW, Latta MA. Rock surface hardness as an indication of exposure age: an archaeological application of the Schmidt Hammer. Archaeometry. 2000;42(1):209–23.
11. Mol L, Viles HA. The role of rock surface hardness and internal moisture in tafoni development in sandstone. Earth Surf Proc Land. 2012;37(3):301–14.
12. Viles H, Goudie A, Grab S, Lalley J. The use of the schmidt hammer and equotip for rock hardness assessment in geomorphology and heritage science: a comparative analysis. Earth Surf Proc Land. 2011;36(3):320–33.
13. Campbell O, Blenkinsop T, Gilbert O, Mol L. Surface and subsurface damage caused by bullet impacts into sandstone. Geosciences. 2021;11(9):395.
14. Campbell O, Blenkinsop T, Gilbert O, Mol L. Bullet impacts in building stone excavate approximately conical craters, with dimensions that are controlled by target material. Sci Rep. 2022;12(1):17634.
15. Open Street Map. Bath City, Maptiler 2022. http://www.openstreetmap.org.
16. Aoki H, Matsukura Y. A new technique for non-destructive field measurement of rock-surface strength: an application of the Equotip hardness tester to weathering studies. Earth Surf Proc Land. 2007;32(12):1759–69.

17. Mccarroll D. The schmidt hammer, weathering and rock surface roughness. Earth Surf Proc Land. 1991;16:477–80.
18. Alberti AP, Gomes A, Trenhaile A, Oliveira M, Horacio J. Correlating river terrace remnants using an Equotip hardness tester: an example from the Miño River, northwestern Iberian Peninsula. Geomorphology. 2013;192:59–70.
19. Coombes MA, Feal-Pérez A, Naylor LA, Wilhelm K. A non-destructive tool for detecting changes in the hardness of engineering materials: application of the Equotip durometer in the coastal zone. Eng Geol. 2013;167:14–9.
20. Wilhelm K, Viles H, Burke Ó. Low impact surface hardness testing (Equotip) on porous surfaces—advances in methodology with implications for rock weathering and stone deterioration research. Earth Surf Proc Land. 2016;41(8):1027–38.
21. Verwaal W, Mulder A. Estimating rock strength with the Equotip hardness tester. In: Verwaal W, editor. International Journal of Rock Mechanics and Mining Sciences and Geomechanics Abstracts, vol. 30. Amsterdam: Elsevier; 1993. p. 659–62.
22. Hack HRGK, Hingira J, Verwaal W. Determination of discontinuity wall strength by Equotip and ball rebound tests. In: Hack HRGK, Hingira J, Verwaal W, editors. International Journal of Rock Mechanics and Mining Sciences & Geomechanics Abstracts, vol. 30. Amsterdam: Elsevier; 1993. p. 151–5.
23. Hansen CD, Meiklejohn KI, Nel W, Loubser MJ, Van der merwe BJ,. Aspect-controlled weathering observed on a blockfield in dronning maud land, antarctica. Geogr Ann: Ser A Phys Geogr. 2013;95(4):305–13.
24. Goggin DJ. Geologically-sensible modelling of the spatial distribution of permeability in eolian deposits: Page Sandstone(Jurassic), northern Arizona. Austin: Univ. of Tex; 1988. p. 463.
25. Filomena CM, Hornung J, Stollhofen H. Assessing accuracy of gas-driven permeability measurements: a comparative study of diverse Hassler-cell and probe permeameter devices. Solid Earth. 2014;5(1):1–11.
26. McPhee C, Arthur K. Klinkenberg permeability measurements: problems and practical solutions. In: Proceedings of the Second Society of Core Analysts European Core Analysis Symposium; UK. 1991; 32(5): 616–7.
27. Gilbert O, Mol L, Campbell O, Blenkinsop T. Permeability and surface hardness surveying of stone damaged by ballistic impact. Heritage. 2019;2(2):1369–89.
28. Aumond P, Can A, Mallet V, De Coensel B, Ribeiro C, Botteldooren D, et al. Kriging-based spatial interpolation from measurements for sound level mapping in urban areas. J Acoust Soc Am. 2018;143(5):2847.
29. Can A, Dekoninck L, Botteldooren D. Measurement network for urban noise assessment: comparison of mobile measurements and spatial interpolation approaches. Appl Acoust. 2014;83:32–9.
30. Chandan KS, Yashwant BK. Optimization of groundwater level monitoring network using GIS-based geostatistical method and multi-parameter analysis: a case study in Wainganga Sub-basin. India Chin Geogr Sci. 2017;27(2):201–15.
31. Goovaerts P, Webster R, Dubois JP. Assessing the risk of soil contamination in the swiss jura using indicator geostatistics. Environ Ecol Stat. 1997;4:49–64.
32. Fitzner B, Heinrichs K, Damage index for stone monuments. Protection and Conservation of the Cultural Heritage of the Mediterranean Cities. Proceedings of the 5th International Symposium on the Conservation of Monuments in the Mediterranean Basin, Sevilla, Spain. Swets & Zeitlinger: Lisse. 2000:315–326.
33. Vergès-Belmin V. ICOMOS-ISCS: illustrated glossary on stone deterioration patterns (English-Chinese version). Xi'an: Shanxi Xinhua Publishing Media Group; 2019.
34. Tucker ME. Blue Bath stone: the real colour of Bath oolite (middle Jurassic, England). J Bath Geol Soci. 2023;41:9–11.
35. Wang HF, Ge C, Zheng YF. Impact response of active damaged materials. Beijing: Beijing Institute of Tecnology Press; 2020.
36. Yang Z. High energy materials and high efficiency damage technology. Beijing: Chemical Industry Press; 2012.
37. Gomez-Heras M, McCabe S, Smith BJ, Fort R. Impacts of fire on stone-built heritage. J Archit Conserv. 2009;15(2):47–58.
38. Mol L, Grenfell M. Influence of landscape moisture sources and topography on rock weathering patterns associated with wildfire. Earth Surf Proc Land. 2022;47(7):1761–77.
39. Sheng GH, Jin SJ, Li C, Bai Q, Wang XY. Compressive-tensile mechanics and energy consumptions of a cementitious composite with high utilization of steel slag. KSCE J Civ Eng. 2023;27(3):1236–48.
40. Wang XY, Liu P, Xu G. Influence of grass lawns on the summer thermal environment and microclimate of heritage sites: a case study of Fuling mausoleum. China Herit Sci. 2021;9:7.
41. Wang XY, Wang J, Wang JH, Sheng GH. Experimental and numerical simulation analyses of flame spread behaviour over wood treated with flame retardant in ancient buildings of fuling mausoleum. China Fire Technol. 2022;7:1–25.
42. Guo QL, Wang XD, Yang SL, Li ZX. Study on the source of water and salt in the mural diseases of dunhuang mogao grottoes. Beijing: Science Press; 2016.
43. Li HS. A study on the features of stone deterioration in stone monuments and their assessment methods. Beijing: Cultural Relics Press; 2014.
44. Sanjurjo-Sánchez J, Alves C, Vidal Romani JR. Assessing the weathering of granitic stones on historical urban buildings by geochemical indices. Earth Sci Res J. 2016;20(3):1.
45. Mackenzie FT, Kump LR. Reverse weathering, clay mineral formation, and oceanic element cycles. Science. 1995;270(27):586.
46. Rahman S. Reverse weathering reactions in marine sediments. In: Cochran JK, Bokuniewicz HJ, Yager PL, editors. Encyclopedia of ocean sciences (third edition). Oxford: Academic Press; 2019. p. 216–27.
47. Chen X, Du S, Zhao L, Yang B, Zhou Q. Effect of stefan flow on the drag force in flow past random arrays of spheres. Chem Eng J. 2021;412: 128691.
48. Lupo G, Niazi Ardekani M, Brandt L, Duwig C. An immersed boundary method for flows with evaporating droplets. Int J Heat Mass Transf. 2019;143: 118563.

Publisher's Note